Numerical evaluation of tree canopy shape near noise barriers to improve downwind shielding

T. Van Renterghem[a] and D. Botteldooren
Department of Information Technology, Ghent University, Sint-Pietersnieuwstraat 41, B-9000 Gent, Belgium

(Received 9 August 2007; revised 16 November 2007; accepted 21 November 2007)

The screen-induced refraction of sound by wind results in a reduced noise shielding for downwind receivers. Placing a row of trees behind a highway noise barrier modifies the wind field, and this was proven to be an important curing measure in previous studies. In this paper, the wind field modification by the canopy of trees near noise barriers is numerically predicted by using common quantitative tree properties. A realistic range of pressure resistance coefficients are modeled, for two wind speed profiles. As canopy shape influences vertical gradients in the horizontal component of the wind velocity, three typical shapes are simulated. A triangular crown shape, where the pressure resistance coefficient is at maximum at the bottom of the canopy and decreases linearly toward the top, is the most interesting configuration. A canopy with uniform aerodynamic properties with height behaves similarly at low wind speeds. The third crown shape that was modeled is the ellipse form, which has a worse performance than the first two types, but still gives a significant improvement compared to barriers without trees. With increasing wind speed, the optimum pressure resistance coefficient increases. Coniferous trees are more suited than deciduous trees to increase the downwind noise barrier efficiency.
 [DOI: 10.1121/1.2828052]

PACS number(s): 43.28.Fp, 43.50.Gf, 43.28.Js [VEO] Pages: 648–657

I. INTRODUCTION

The screen-induced refraction of sound by wind is a well-known problem,[1–3] resulting in a reduced shielding efficiency of noise barriers in case of downwind sound propagation. The use of a row of trees behind noise barriers was shown to be an interesting solution to improve noise shielding from highways. In Ref. 4, a wind tunnel study at scale showed that changing the wind field near noise barriers by using synthetic windbreaks limits the negative effects of the wind to an important degree. In a monitoring campaign along a highway,[5] the positive effect of a row of trees behind a noise barrier was proven experimentally. Simultaneous noise recordings were made behind part of a long noise barrier with and without trees. In this way, the reduction in screen-induced refraction of sound was measured directly. The (downwind) microphone behind the trees yielded lower total A-weighted sound pressure levels resulting from traffic noise and this difference in levels increased with increasing wind speed. For a wind speed of 10 m/s at a height of 10 m above the ground, an increased shielding of about 4 dBA was observed due to the presence of the trees.[5] In case of (strong) upwind sound propagation, the measured effect of the presence of the trees was very limited.[5]

In Refs. 6 and 7, a numerical model was developed for this type of sound propagation problems, involving complex wind flows. The model was validated with success for the situations measured in the wind tunnel study.[4] Further, additional calculations were performed to find important parameters in situations where noise barriers and trees are combined. The focus was on noise barriers on either side of the acoustic source. The magnitude of the incident wind speed, the distance between the source and the noise barriers, the location and the height of the wind reducing structures, as well as the influence of the porosity of the windbreaks were studied. The properties of synthetic windscreens were used to simulate the wind field near noise barriers and trees. Measured pressure drops as a function of flow velocity, for screens with different porosities, were used for these calculations.

Practical recommendations concerning the type of trees that should be used behind noise barriers are however hard to derive from this previous study. For flat windscreens, the optical porosity (i.e., the percentage of open space as seen perpendicularly to the windscreen side) is sufficient to describe its aerodynamic properties.[8] In the case of a tree shelterbelt, two shelterbelts with similar optical porosities may have a very different arrangement of plant elements, different vegetative surface areas and volumes, and a different amount of open spaces within their canopies.[8] It can therefore be concluded that optical porosity is not a good measure to describe the wind flow through the canopies of real trees. This means that the results from the numerical predictions made in Ref. 6 cannot be translated directly to practice.

The calculations in Ref. 6 are further based on windscreens with a uniform porosity. In general, a large variation in the aerodynamic properties of the crown of trees with height is possible. Canopy shape was shown to be an important factor when looking at ground deposed particles in air quality modeling.[9] Changing the wind reducing properties of the canopy as a function of height will result in signifi-

[a]Author to whom correspondence should be addressed. Electronic mail: timothy.van.renterghem@intec.ugent.be

cantly altered wind fields. It is therefore interesting to study the influence of canopy shape on the refraction of sound near noise barriers.

This paper is organized as follows. In Sec. II, the simulation of the flow field near noise barriers in combination with trees is considered. Section II A discusses briefly how atmospheric boundary layer flows can be modeled accurately. In Sec. II B, the effect exerted by the canopy of trees on the wind flow is considered, and it is shown how this can be simulated within standard computational fluid dynamics (CFD) software. Section III discusses briefly the numerical model to simulate sound propagation near the noise barrier, and an overview of model parameters is given. In Sec. IV, numerical results are presented and discussed and in Sec. V, conclusions are drawn.

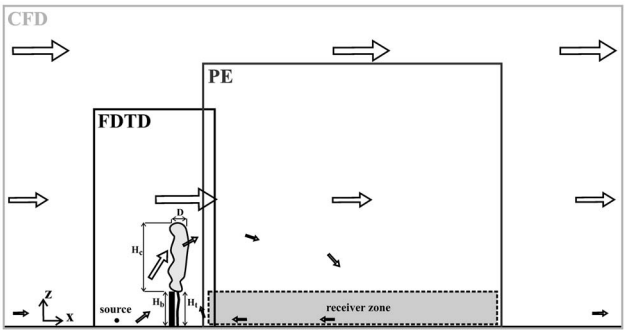

FIG. 1. Overview of the simulation areas, indicating the CFD, FDTD, and PE area. H_b indicates the barrier height, H_t the tree trunk height, H_c the canopy height, and D indicates the width of the canopy. The arrows give an indication of the wind direction and its magnitude near the noise barrier in combination with trees. The receiver zone is shown as well.

II. NUMERICAL SIMULATION OF FLOW FIELD

A. Atmospheric boundary layer flows

The two-dimensional velocity fields near the noise barriers are calculated with the CFD software FLUENT 6.3.[10] The Reynolds-averaged Navier–Stokes equations are solved by applying a standard $k-\varepsilon$ turbulence model. This "turbulence closure" model is widely applied in engineering applications, and is sufficiently accurate for the current application. Turbulent effects are introduced by means of two additional equations to quantify the turbulent kinetic energy and its dissipation rate. Accurate modeling of vertical gradients in the horizontal wind velocity component is of main concern. Predicted values of turbulent parameters are not of interest in the current application.

Vertical profiles of the horizontal wind velocity u_x, turbulent kinetic energy k, and turbulence dissipation rate ε need to be set at the upstream boundary condition. The following equations apply to a neutral, atmospheric boundary layer in equilibrium:[11]

$$u_x = \frac{u_*}{\kappa} \ln\left(1 + \frac{z}{z_0}\right), \tag{1}$$

$$k = \frac{u_*^2}{\sqrt{C_\mu}}, \tag{2}$$

$$\varepsilon = \frac{u_*^3}{\kappa(z + z_0)}, \tag{3}$$

where u_* is the friction velocity, κ is the Von Karman constant (equal to 0.4), z is the height above ground level, and z_0 is the aerodynamic roughness length. C_μ is a model constant of the $k-\varepsilon$ model which is parameterized by measurements. It relates k and ε to the turbulent dynamic viscosity μ_t by the following relation:

$$\mu_t = C_\mu \rho \frac{k^2}{\varepsilon}, \tag{4}$$

where ρ is the mass density of air. The value of C_μ is usually set to 0.09.[11]

The flow simulations are performed for friction velocities of 0.4 and 0.8 m/s. The aerodynamic roughness length equals 0.01 m. These parameters fully define the inflow boundary conditions when using Eqs. (1)–(3). The dimensions of the two-dimensional simulation domain are expressed relative to the total length of the flow disturbing structures L, which is equal to the noise barrier height H_b plus the part of the canopy extending above the noise barrier. In the present simulations, the tree trunk height H_t is equal to H_b, whereas the canopy height H_c equals $2H_t$. As a consequence, L equals $3H_b$ (see Fig. 1). Boundary conditions are imposed at sufficient distances from the flow disturbing structures. The height of the computational grid is $25L$. A region of $9L$ upstream and $34L$ downstream from the noise barrier is modeled. Along the length of the top boundary condition, constant values of horizontal velocity, turbulent kinetic energy, and its dissipation rate are imposed, based on the values of the inlet conditions at this height. The outflow boundary condition of FLUENT[10], assuming that there are no stream-wise gradients, is used at the right-hand side of the grid. The recommendation given in Ref. 12, concerning accurate flow simulations in the atmospheric boundary layer, are followed.

B. Flow field near trees

The presence of a canopy—or any windbreak—has a significant effect on the flow field. Such structures exert a drag force on the wind field, causing a net loss of momentum in the (incompressible) flow. When the permeability of the windbreak decreases, the so-called "bleed flow" through the windbreak decreases and the drag force increases. This is accompanied by a stronger upward deflection of the approach flow.

The airflow through the canopy of trees results in a pressure drop. The pressure resistance coefficient k_r is a commonly used measure to quantify this pressure drop, and is defined as follows:

$$\Delta p = k_r \frac{\rho u_x^2}{2}. \tag{5}$$

The pressure resistance coefficient can be related to physical characteristics of the canopy of trees. When assuming that the aerodynamic drag of the canopy balances the pressure drop, one may write, following Ref. 13:

$$k_r \approx \int_0^D C_d \,\mathrm{LAD}\, dx, \tag{6}$$

where D is the width of the canopy layer in horizontal direction, C_d is the dimensionless drag coefficient of the elements of the canopy, and LAD is the leaf area density. The LAD is defined as the total area of leafs per unit volume of the canopy.

Drag coefficients of trees are independent of the wind speed encountered outdoors near ground level.[14] Information concerning the drag coefficient of different types of trees can be found in literature. Values for individual deciduous trees range from 0.15 to 0.25.[15–18] A value of 0.2 is commonly used in numerical studies of wind flow through forests. In Ref. 14, drag coefficients were measured for single-row deciduous "windbreak" species. Most values are near 0.5. Coniferous types of trees are characterised by somewhat larger values (0.6–1.2).[14]

The LAD or the equivalent needle area density (NAD) for conifers, is a common measure in quantitative plant research. As trees can form extremely diverse crown shapes, the LAD or NAD may depend largely on height. The crown form is not only dependent of the species, but also on the local topography, climate, the availability of nutrients, etc. The difference between isolated trees and trees in a dense tree population can be large as well.[9] A typical value of the maximum LAD of the canopy of deciduous trees is 1 $m^2\ m^{-3}$,[18] however large deviations from that value appear. The NAD is usually larger. In Refs. 19 and 20, maximum values of 2 $m^2\ m^{-3}$ were found.

The canopy width D depends on the height as well, and has a maximum value typically in the order of a few meters for a single row of trees. Assuming that the LAD and C_d are constant in horizontal direction, Eq. (6) becomes:

$$k_r \approx C_d \,\mathrm{LAD}\, D. \tag{7}$$

In the remainder of this paper, k_r will be used as an independent variable, and is representative for a variety of combinations of the drag coefficient, the LAD, and the canopy width, as governed by Eq. (7).

A velocity-dependent pressure drop over a plane can be modeled in FLUENT[10] by using the porous jump boundary condition. The pressure drop over this plane represents the total pressure drop as caused by the air flow through the canopy. The resistance coefficient can be made dependent on height to account for vertical changes of LAD.

Three different crown shapes were considered. The barrier height H_b and the trunk height H_t equal 4 m, and the canopy height H_c equals 8 m. A first canopy type has uniform aerodynamic properties with height, and is further indicated as "uniform." This type of canopy form is representative for, e.g., a dense hedge. A second type has a maximum pressure resistance coefficient near the top of the noise barrier (or at the bottom of the canopy) and a linear decrease towards the top of the canopy. This type is further indicated as "triangle," and is typical for conifers. A third canopy type which is considered has an ellipse-like form, with a maximum k_r near the middle of the canopy, and large gradients in k_r near the top and bottom of the crown. This type is further indicated as "ellipse," and is representative for common deciduous trees. The sum of k_r over the total canopy height is kept the same for these three crown forms. This allows investigating the importance of the distribution of the aerodynamic properties over height. An overview of k_r with height for these crown types is given in Fig. 2, for an average k_r equal to 1.

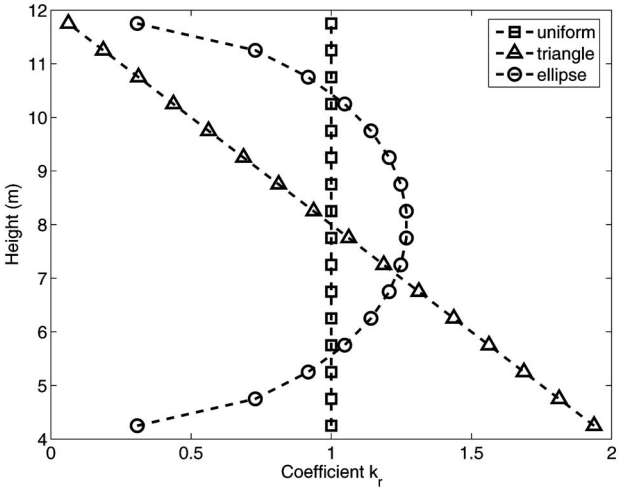

FIG. 2. The pressure resistance coefficient k_r for the three types of crown shapes (uniform, triangle, and ellipse) used for the numerical calculations in this paper. The average values of k_r equal 1.

Numerical calculations are performed for average values of k_r equal to 1, 2, and 4, for the three crown shapes considered. Note that k_r is the product of the drag coefficient, leaf area density, and canopy width. The values used in the calculations cover a wide variety of realistic situations. A specific canopy form is prescribed in a vertical resolution of k_r equal to 0.5 m.

III. SOUND PROPAGATION MODEL

The acoustic calculations are performed with the finite-difference time-domain (FDTD) method, coupled to the parabolic equation (PE) method.[21] Two-dimensional calculations are performed, implying a coherent line source, and infinitely long noise barriers with constant cross sections. Traffic, which is the prominent source when looking at noise barriers, is however more accurately modeled as an incoherent line source. When looking at noise barrier efficiency at individual frequencies, significant differences are observed when comparing calculations made with a coherent and incoherent line source.[22] When averaging to octave bands, as will always be done in this paper, differences become much smaller. An approach such as the one proposed in Ref. 22 cannot be used as the propagation medium is moving. The large number of three-dimensional calculations needed to simulate an incoherent line source more accurately would lead to huge computing times. Nevertheless, the difference between a coherent and incoherent line source on the main quantity used in this paper, namely the tree effect (see Sec. IV for its definition), is expected to be limited.

The FDTD method, solving the moving-medium sound propagation equations,[23,7,24] is used in the direct vicinity of

the noise barrier. An overview of the different regions of the simulation domain, with the corresponding numerical method, is shown in Fig. 1. The stationary flow field as calculated by the CFD software is used as a so-called background flow. This implies that refraction of sound by wind is accounted for accurately, but the acoustic waves do not influence the ambient flow, and generation of sound by wind is not considered. These two latter effects are however not important in the current application. Upward directed flows very close to the barrier and trees are accounted for. Perfectly matched layers are applied at the left, right, and top boundaries of the FDTD computational domain, to simulate an unbounded atmosphere. More information on the numerical schemes is given in the following. In absence of flow, the efficient staggered spatial and staggered temporal grid is used.[25] In a moving medium, staggered-in-space calculations are combined with the prediction-step staggered in time (PSIT) approach.[26] Such a scheme was shown to be an interesting compromise between accuracy, numerical stability, and computational efficiency.[26] Further, flow velocities and propagation distances in the FDTD region are sufficiently low to perform accurate calculations with the PSIT scheme.

The Green's function PE (GFPE) method[27,28] is used to model sound propagation from the source region to the receivers. The GFPE calculations start from a column of complex pressures, derived from the FDTD domain. Refraction is modeled using the effective sound speed approach. A horizontal flow with range-dependent wind speed profiles is assumed. This is a good approximation at sufficient distance behind the noise barrier. On top of the computational PE domain, an absorbing layer was placed.

Combining FDTD in the source region with GFPE downwind from the noise barrier allows modeling the effects of the complex flow field near the source, barrier, and trees accurately, but explores at the same time the efficiency of the GFPE method for the longer distance part of the outdoor sound propagation problem. This hybrid model was shown to be computationally very efficient, without resulting in loss of accuracy. Details concerning the coupling between FDTD and PE can be found in Ref. 21.

The noise barrier height H_b equals 4 m. The noise barrier thickness equals 0.1 m. The source is placed at $2H_b$ upwind from the barrier, at a height of 0.30 m. The PE calculations start at $1H_b$ downwind from the barrier, and continue until $35H_b$. The noise barrier and the ground in the FDTD region are modeled as rigid planes, whereas in the PE region both a rigid ground and grass-covered ground is modeled. For the latter, the common Delany and Bazley model[29] is used, with an effective flow resistivity equal to 200 kPa s/m^2. Downwind sound propagation is considered, for two incident wind speed profiles, characterized by friction velocities of 0.4 and 0.8 m/s (see Sec. II A).

Scattering of sound on tree elements is not considered in this paper as this is mainly a high-frequency phenomenon. Measurements behind a noise barrier with and without deciduous trees, in the absence of wind, showed that below 1.5 kHz, scattering is smaller than 1 dB.[6] At 10 kHz, a difference of 6 dB was measured.[6] Traffic however produces only a small amount of acoustic energy in this high frequency range relative to low frequency bands. So the contribution of this scattered sound to the total A-weighted sound pressure levels is small.[6] This conclusion was confirmed by several authors. In Ref. 30, it was concluded that roadside trees do not significantly influence traffic noise at ground level. Even belts of trees of several tens of meters result in only little attenuation for traffic noise.[31] Martens states that the foliage of trees can be seen as a low-pass filter: The frequencies of the dominant peaks in traffic noise are too low to be amplified or weakened.[32]

The presence of a noise barrier in wind results in an increase in turbulence compared to the amount of turbulence observed over unobstructed ground. This can cause scattering of sound into the shielded area, thereby reducing the noise barrier efficiency. Downwind sound propagation calculations through screen-induced turbulence, for a similar configuration as the one considered in this paper, were performed for a sound frequency of 500 Hz in Ref. 33. It was shown that turbulent scattering results in fluctuations in the noise level in the shielded region up to 3 dB at 250 m from the source. The time-averaged effect, on the other hand, was only of the order of 0.2 dB. Therefore, it was concluded that screen-induced turbulence could be neglected when looking at average noise levels.

The main interest in this study is in shielded traffic noise. Therefore, calculations up to the octave band of 1000 Hz are sufficient. The maximum frequency to be considered is 1405 Hz, and lies within the 1 dB region for scattering. The octave bands with center frequencies 63, 125, 250, 500, and 1000 Hz are used in the analysis. To calculate the energetically average sound pressure level in each octave band, 15 frequencies are considered.

The following computational parameters were used. The FDTD spatial discretization step was 0.02 m in both dimensions. This led to more than ten cells per wavelength for the highest frequency considered. The temporal discretization step was 40 μs, and 5000 time steps were sufficient to build the PE starting fields ranging from ground level until 40 m. The perfectly matched layers at the boundaries of the domain consisted of 40 computational cells. A broadband Gaussian pulse was emitted at the source position. For the PE calculations, ten computational cells per wavelength were used in vertical direction. The horizontal propagation step was equal to a single wavelength, in order to have sufficient spatial resolution when plotting sound pressure fields and to accurately account for the rapid changes of the wind speed profiles in the lee of the barrier. At each propagation step, the wind speed profile was updated. The thickness of the PE damping layer was 150 times the wavelength. To avoid spatial interpolation while calculating octave band values, the spatial parameters of the PE calculation were kept constant for each of the 15 frequencies in the octave band considered and corresponded to the highest frequency in that band.

IV. RESULTS AND DISCUSSION

The zone of interest for quieting (i.e., the receiver zone, see Fig. 1) extends in horizontal direction from $1H_b$ to $35H_b$, and in vertical direction from ground level up to $1H_b$. Dis-

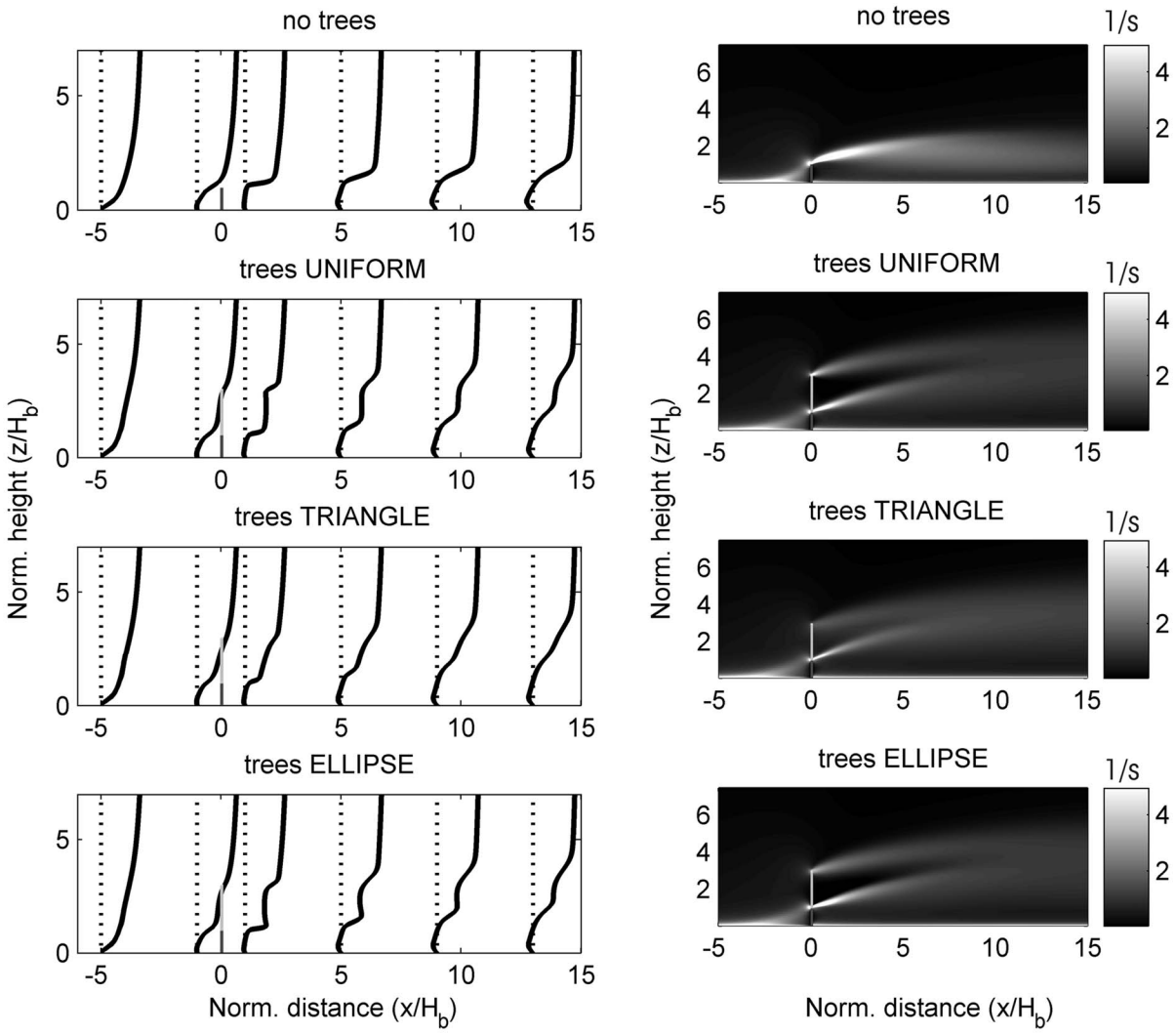

FIG. 3. In the left-hand column, vertical profiles of the horizontal component of the wind speed are shown at selected locations. In the right-hand column, the corresponding fields of vertical gradients in the horizontal wind speed are presented. Only positive gradients are shown. Distances and heights are expressed relative to the noise barrier height H_b, which equals 4 m. The first row of figures shows the fields when no trees are present near the noise barrier. In the second row, the uniform canopy shape, in the third row the triangular form, and in the last row the ellipse shape is considered. The average values of k_r equal 2. The incident friction velocity u_* equals 0.8 m/s.

tances and heights are expressed relative to the noise barrier height, but this does not imply that scaling is possible for the calculations performed in this study. The results will be presented as contour plots of sound levels, as sound levels along a horizontal line at a fixed height, or as histograms indicating the fraction of the area of the receiver zone falling within a certain sound level class. A bin increment of 1 dB will be used in the histograms. Full octave band sound pressure levels are considered. To limit the number of contour plots, only the octave bands with center frequency 125 and 1000 Hz are shown. These frequency bands are representative for respectively the engine noise and tire-road noise peaks in typical traffic spectra.[34]

The insertion loss IL is defined as the sound pressure level in absence of a noise barrier, minus the sound pressure level in presence of a barrier, for the same source receiver configuration. The screen-induced refraction of sound by wind SIROS is the sound pressure level with the noise barrier in the presence of wind, minus the sound pressure level with the noise barrier in absence of wind, for the same source-noise barrier–receiver configuration. A third quantity that will be used is the tree effect TE, which is defined as the sound pressure level in the presence of a noise barrier and wind, minus the sound pressure level in the presence of a noise barrier combined with trees and wind, for the same source–noise barrier–receiver configuration. The following equations give an overview of the definitions of IL, SIROS, and TE:

$$\mathrm{IL} = L_{p,\text{no barrier,no trees,no wind}} - L_{p,\text{barrier,no trees,no wind}}, \quad (8)$$

$$\mathrm{SIROS} = L_{p,\text{barrier,no trees,wind}} - L_{p,\text{barrier,no trees,no wind}}, \quad (9)$$

$$\mathrm{TE} = L_{p,\text{barrier,no trees,wind}} - L_{p,\text{barrier,trees,wind}}. \quad (10)$$

Positive values of IL indicate that the noise barrier is effective in reducing sound pressure levels in absence of wind. Positive values of SIROS indicate that the wind reduces the

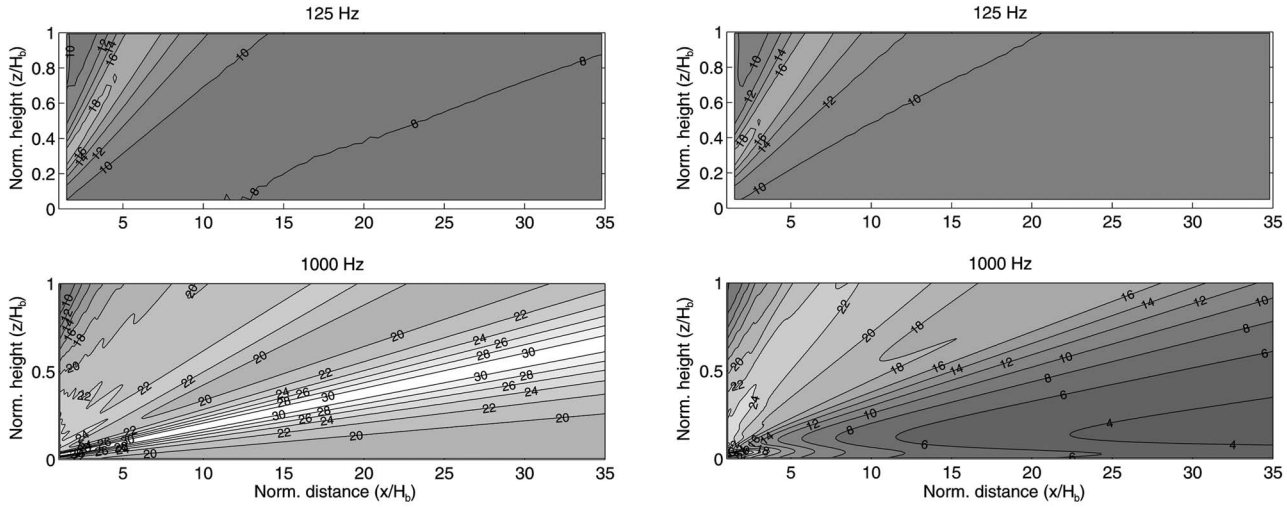

FIG. 4. Contour plots of IL (insertion loss) for the octave bands with center frequencies 125 and 1000 Hz. The noise barrier height H_b equals 4 m. On the left, a rigid ground is assumed downwind from the noise barrier. Plots on the right correspond to a grass-covered ground downwind from the noise barrier.

barrier efficiency. Positive values of TE indicate that the presence of trees increases shielding when there is wind, or alternatively, part of the SIROS is counteracted.

Vertical gradients in the horizontal component of the wind speed determine the magnitude of the screen-induced refraction of sound in the shielded area. In Fig. 3, profiles of the horizontal wind component are shown at selected locations near the noise barrier, and near the noise barrier in combination with the different canopy shapes. Fields plots of positive, vertical gradients in the horizontal wind speed are shown as well. The friction velocity of the inflow boundary condition was 0.8 m/s, and an average value of k_r equal to 2 is used. In absence of trees, large positive gradients in the wind speed are observed starting from the top of the noise barrier, stretching in downwind direction. In the presence of trees, the downwind area with large positive gradients is significantly reduced. Near the top of the trees however, additional gradients appear. Such gradients are most prominent in case of uniform canopy properties with height. The triangular tree shape, on the other hand, induces a smooth transition between the top region of the canopy and the undisturbed region outside the canopy, resulting in smaller gradients at the tree top. The gradients near the top of the barrier are most significantly reduced in case of the triangle crown shape: the maximum values of k_r are found just near the noise barrier top. These barrier-top gradients are somewhat larger for the ellipse form than for the uniform canopy.

In the case of a friction velocity equal to 0.4 m/s, similar conclusions could be drawn. The maximum gradients that are found near the top of the noise barrier and the top of the canopy stay more or less the same. However, the region with positive gradients is much smaller, and only appears close to the barrier and trees.

Contour plots of IL (in absence of wind) in the receiver zone are shown in Fig. 4, for a rigid and grass-covered ground. With increasing octave band center frequency, the IL

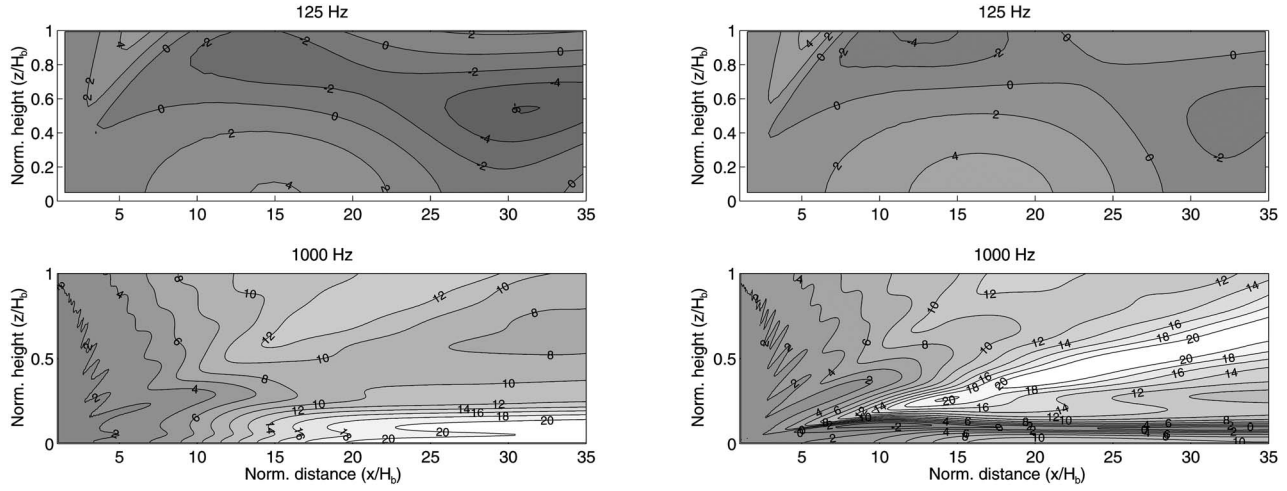

FIG. 5. Contour plots of SIROS (screen-induced refraction of sound by wind) for u_*=0.8 m/s. The octave bands with center frequencies 125 and 1000 Hz are shown. The noise barrier height H_b equals 4 m. On the left, a rigid ground is assumed downwind from the noise barrier. Plots on the right correspond to a grass-covered ground downwind from the noise barrier.

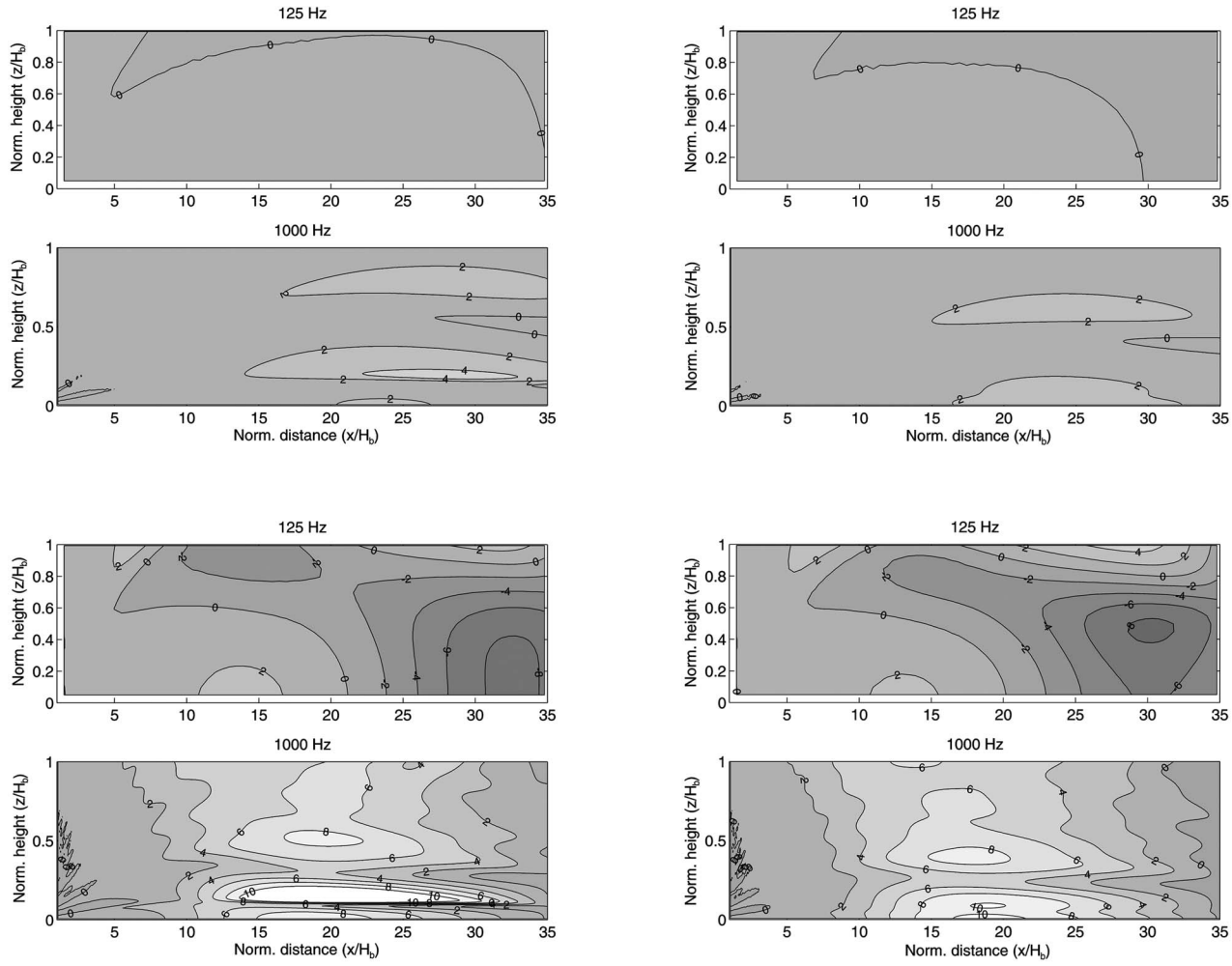

FIG. 6. Contour plots of TE (tree effect). The panels above are for $u_*=0.4$ m/s, the panels below for $u_*=0.8$ m/s. The octave bands with center frequencies 125 and 1000 Hz are shown. The noise barrier height H_b equals 4 m. On the left, a rigid ground is assumed downwind from the noise barrier. Plots on the right correspond to a grass-covered ground downwind from the noise barrier. A triangle crown shape is used, with $k_r=2$.

becomes larger. For the low frequencies, the differences between rigid ground and grass-covered ground are small. For the higher frequencies, the IL in case of a softer ground is smaller, and this is very significant for the octave band with center frequency 1000 Hz: A large zone with values for the IL lower than 5 dB is observed. This is explained by the reduction of the positive influence of soft ground on propagation from this low lying source by the presence of the noise barrier.

Contour plots of SIROS, in case of a friction velocity of 0.8 m/s, are shown in Fig. 5. For the octave band of 63 Hz, refraction is limited. For the octave band of 125 Hz, values of SIROS are negative at some locations, indicating that the wind results in a (limited) decrease of the sound pressure level.

For higher frequencies, values for SIROS are larger and mainly positive. At 1000 Hz, values exceed 10 dB starting from about $15H_b$ downwind from the noise barrier, and maximum values found in the region of interest are larger than 20 dB. In case of the rigid ground, and especially for the octave band of 250 Hz, zones of negative SIROS are still found. This is caused by a shift in the location where conditions for destructive interference are met.

Contour plots of TE are shown in Fig. 6, in case of a friction velocity of 0.4 and 0.8 m/s, and for a rigid ground and grass-covered ground. A triangular crown shape is considered, equivalent to a uniform canopy with $k_r=2$. The influence of the trees is very small at the octave band with center frequency 63 Hz, as screen-induced refraction of sound is limited as well.

For the lower wind speed ($u_*=0.4$ m/s), the wind modification by the trees has a significant effect starting from the octave band of 250 Hz. In case of a rigid ground, maximum effects exceed 5 dB starting from 500 Hz. For the softer ground, maximum effects are somewhat smaller, but zones with negative TE are hardly present.

For the higher wind speed ($u_*=0.8$ m/s), the maximum values, either positive or negative, are much larger. The maximum improvements by the presence of trees in a wind situation now exceed 10 dB starting from 250 Hz. Large zones with positive effects, over the full height of the receiver zone, are found for the octave bands of 500 and 1000 Hz. The region of significant improvement is found roughly between $10H_b$ and $30H_b$ downwind from the noise

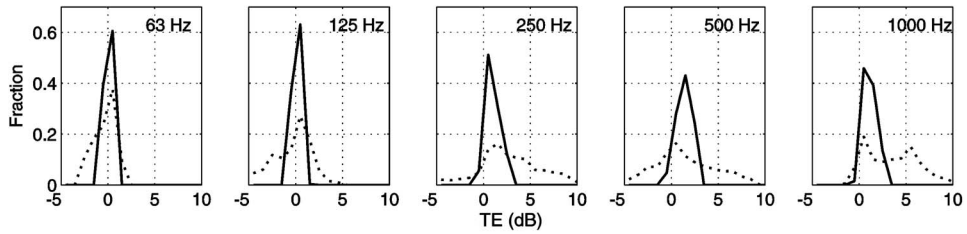

FIG. 7. Distribution of TE over decibel classes in the receiver zone, for a noise barrier height H_b which equals 4 m. Friction velocities of 0.4 m/s (full lines) and 0.8 m/s (dotted lines) are considered. The octave bands with center frequencies 63, 125, 250, 500, and 1000 Hz are shown. A grass-covered ground is assumed downwind from the noise barrier. A triangle crown shape is used, with $k_r=2$.

barrier. The difference between a rigid ground and grass-covered ground becomes small, especially at 500 and 1000 Hz.

The histograms in Fig. 7 clarify the results. The distribution of the area in the receiver zone over TE classes becomes broader with increasing wind speed. At 125 Hz, large zones with negative TE are found, for both ground types. The fraction of the receiver zone with negative values decreases with frequency, and at 1000 Hz only positive effects are found. This is observed for both wind speeds.

In the histograms in Fig. 8, a comparison is made between the TE for the different tree forms, for $u_*=0.4$ and 0.8 m/s. The average values of k_r are equal to 2 in all cases. For a friction velocity of 0.4 m/s, significant differences between the different crown shapes are observed, starting from the octave band of 250 Hz. The uniform and triangle shape give quite similar tree effects, which are better than the tree effect for an ellipse shape.

For a friction velocity of 0.8 m/s, only the 1000 Hz octave band seems to be significantly affected by tree form. This is however the dominant frequency band when looking at rolling noise near highways. A similar conclusion can be drawn when looking at the TE along a horizontal line, at a fixed receiver height of 2 and 4 m (see Fig. 9). At the distance where maximum effects are observed, the triangle shape gives an improvement of about 2–3 dB compared to the ellipse form. The uniform canopy shape lies in between the other types.

It can therefore be concluded that the triangular crown shape is the most interesting one, followed by the uniform one. For lower wind speeds, both types behave similarly. The ellipse form has a somewhat worse performance, but still improves the downwind shielding significantly compared to a noise barrier without trees. Maximum values are a few decibels smaller, while negative TE areas are more frequently observed.

The influence of the magnitude of k_r on TE is shown in Fig. 10 for a uniform crown. A grass-covered ground is considered downwind. Numerical predictions are shown for both the low wind speed and high wind speed.

For the low wind speed, uniform trees with $k_r=2$ are a significant improvement over trees with $k_r=1$, at all frequencies. The differences between $k_r=2$ and $k_r=4$ are less pronounced. Below 250 Hz, the difference between them is very limited. Above 250 Hz, $k_r=4$ results only in a limited additional improvement compared to $k_r=2$. It can therefore be concluded that values of k_r larger than 2 do not increase downwind shielding. For the high wind speed, k_r equal to 4 gives a significant improvement over $k_r=2$. Further, the larger the value of k_r, the smaller the fraction of the area of the receiver zone with negative TE, especially at higher frequencies. An asymptotical value is not found for the range of values of k_r that are modeled at the high wind speed. From this analysis, it is clear that conifers are preferred behind noise barriers to improve the downwind shielding, since their typical needle area densities and canopy element drag coefficients lead to larger pressure resistance coefficients. Further, the typical crown form of coniferous trees is close to the triangular canopy shape. In addition, during winter, there is no loss in biomass.

V. CONCLUSIONS

In this paper, the possibilities of modifying the wind field by the canopy of trees near noise barriers, in order to improve downwind shielding, is numerically investigated.

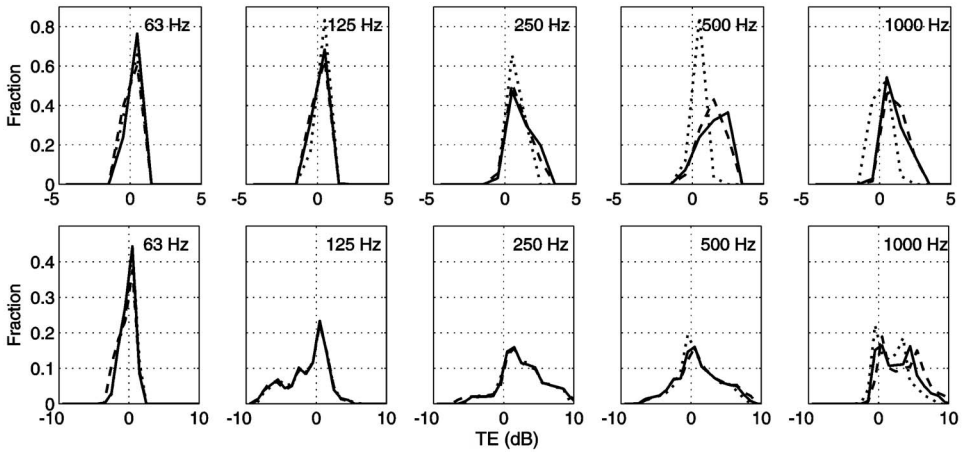

FIG. 8. Distribution of TE over decibel classes in the receiver zone, for a noise barrier height H_b which equals 4 m. The full lines represent uniform canopy, the dashed lines the triangular canopy and dotted lines the ellipse form. Friction velocities of 0.4 m/s (first row) and 0.8 m/s (second row) are considered. A grass-covered ground is assumed downwind. The average values of k_r equal 2.

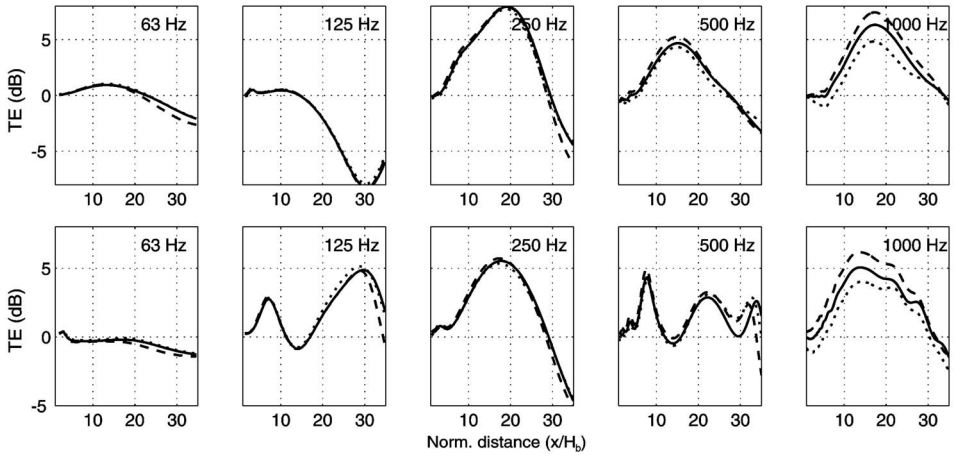

FIG. 9. TE along a horizontal line in the shielded area of the noise barrier, at a fixed height of 2 m (first row) and 4 m (second row). The noise barrier height H_b equals 4 m. The full lines represent uniform canopy, the dashed lines the triangular canopy and dotted lines the ellipse form. A friction velocity of 0.8 m/s is considered, together with an average value of k_r equal to 2. Grass-covered ground is assumed downwind from the noise barrier.

Common (or documented) quantitative tree properties are used to predict wind fields. These are the leaf area density, the canopy element drag coefficient, and the canopy width. The pressure loss coefficient is approximately equal to the product of these three quantities. Scattering on leaves and the effects of turbulence are not taken into account. This choice is justified by considering the rather low frequency interval of importance of shielded traffic noise.

In the configuration under study, a negative effect of wind on the downwind noise barrier shielding efficiency is observed, starting from the octave band with center frequency of 250 Hz. Below 1000 Hz, zones with increased shielding by the action of the wind are possible, because of a shift of the location where conditions for destructive interference are met, especially in case of a rigid ground downwind from the noise barrier. At 1000 Hz, only negative wind effects are found, and their magnitude exceed 20 dB for an incident wind speed profile with a friction velocity of 0.8 m/s.

The triangular crown shape, where the pressure drop is maximum at the bottom of the canopy and which decreases linearly towards the top, is the most interesting configuration. Analysis of the vertical gradients in the horizontal component of the wind speed yielded the smallest values for this configuration, both near the barrier top and the top of the canopy. The second best configuration in this numerical study is a canopy with uniform aerodynamic properties with height. For the low wind speed modeled (friction velocity of 0.4 m/s), both types behave similarly. The ellipse form has a somewhat worse performance, but still improves the downwind shielding significantly compared to a noise barrier without trees. The zone with increased shielding by the presence of trees is located mainly at distances between $10H_b$ and $30H_b$ downwind from the noise barrier (with H_b the noise barrier height). With increasing wind speed, the optimum pressure resistance coefficient increases. For the low wind speed used in this paper, a pressure resistance coefficient equal to 2 is sufficient in case of a uniform canopy. For the high wind speed, a value of 4 gave a significant improvement over a value of 2.

The largest positive and most consistent effects by the presence of the trees in wind are found for the octave band of 1000 Hz. This is the dominant frequency band when looking at noise near highways.

The numerical analysis in this paper leads to the conclusion that coniferous trees are more suited than deciduous trees to improve the wind field near noise barriers. Their typical needle area densities and canopy element drag coefficients lead to larger pressure resistance coefficients. Further, their canopy shape is usually close to the optimal triangular form, and during winter, there is no significant loss in biomass.

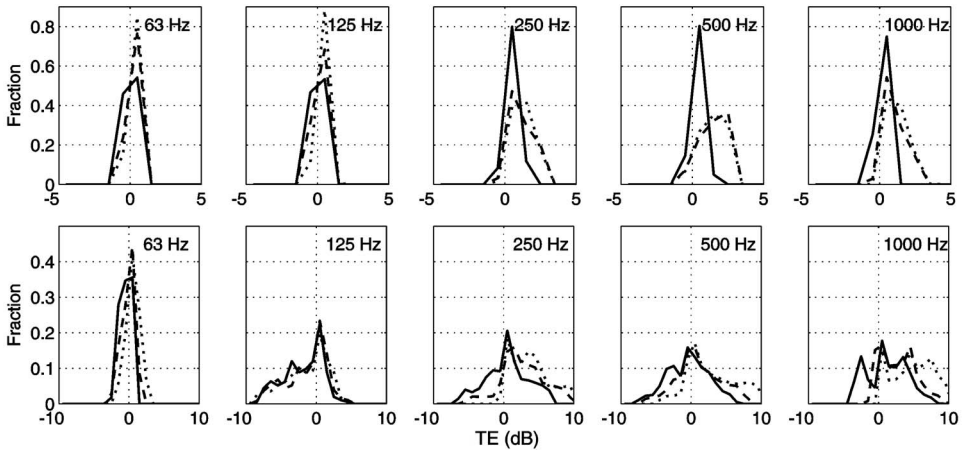

FIG. 10. Distribution of TE over decibel classes, for a friction velocity of 0.4 m/s (first row) and 0.8 m/s (second row). The noise barrier height H_b equals 4 m. The full lines are for $k_r=1$, the dashed lines for $k_r=2$, and the dotted lines for $k_r=4$. A grass-covered ground is assumed. A uniform crown shape is simulated.

[1]R. De Jong and E. Stusnick, "Scale model studies of the effect of wind on acoustic barrier performance," Noise Control Eng. **6**, 101–109 (1976).
[2]K. Rasmussen and M. Arranz, "The insertion loss of screens under the influence of wind," J. Acoust. Soc. Am. **104**, 2692–2698 (1998).
[3]E. Salomons, "Reduction of the performance of a noise screen due to screen-induced wind-speed gradients. Numerical computations and wind tunnel experiments," J. Acoust. Soc. Am. **105**, 2287–2293 (1999).
[4]T. Van Renterghem, D. Botteldooren, W. Cornelis, and D. Gabriels, "Reducing screen-induced refraction of noise barriers in wind by vegetative screens," Acust. Acta Acust. **88**, 231–238 (2002).
[5]T. Van Renterghem and D. Botteldooren, "Effect of a row of trees behind noise barriers in wind," Acust. Acta Acust. **88**, 869–878 (2002).
[6]T. Van Renterghem and D. Botteldooren, "Numerical simulation of the effect of trees on downwind noise barrier performance," Acust. Acta Acust. **89**, 764–778 (2003).
[7]T. Van Renterghem, "The finite-difference time-domain method for simulation of sound propagation in a moving medium," Ph.D. dissertation, University Gent, 2003.
[8]X. Zhou, J. Brandle, C. Mize, and E. Takle, "Three-dimensional aerodynamic structure of a tree shelterbelt: Definition, characterization and working models," Agroforest. Syst. **63**, 133–147 (2005).
[9]J. Donat and B. Ruck, "Simulated ground deposition of fine airborn particles in an array of idealized tree crowns," Boundary-Layer Meteorol. **93**, 469–492 (1999).
[10]FLUENT, *Computational Fluid Dynamics Software*, version 6.3, Fluent, Incorporated, Centerra Resource Park, Lebanon, NH.
[11]P. Richards and R. Hoxey, "Appropriate boundary conditions for computational wind engineering models using the k-ε turbulence model," J. Wind. Eng. Ind. Aerodyn. **46–47**, 145–153 (1993).
[12]B. Blocken, T. Stathopoulos, and J. Carmeliet, "CFD simulation of the atmospheric boundary layer—wall function problems," Atmos. Environ. **41**, 238–252 (2007).
[13]J. Wilson, "Numerical studies of flow through a windbreak," J. Wind. Eng. Ind. Aerodyn. **21**, 119–154 (1985).
[14]L. Hagen and E. Skidmore, "Windbreak drag as influenced by porosity," Trans. ASAE **14**, 464–465 (1971).
[15]H.-B. Su, R. Shaw, K. Pawu, C.-H. Moeng, and P. Sullivan, "Turbulent statistics of neutrally stratified flow within and above a sparse forest from large-eddy simulation and field observations," Boundary-Layer Meteorol. **88**, 363–397 (1998).
[16]Ü. Rannik, T. Markkanen, J. Raittila, P. Hari, and T. Vesala, "Turbulence statistics inside and over forest: Influence of footprint prediction," Boundary-Layer Meteorol. **109**, 163–189 (2003).
[17]M. Irvine, B. Gardiner, and M. Hill, "The evolution of turbulence across a forest edge," Boundary-Layer Meteorol. **84**, 467–496 (1997).
[18]J. Lopes da Costa, F. Castro, J. Palma, and P. Stuart, "Computer simulation of atmospheric flows over real forests for wind energy resource evaluation," J. Wind. Eng. Ind. Aerodyn. **94**, 603–620 (2006).
[19]A. Porté, A. Bosc, I. Champion, and D. Loustau, "Estimating the foliage area of Maritime pine (Pinus pinaster Aït.) branches and crowns with application to modelling the foliage area distribution in the crown," Ann. For. Sci. **57**, 73–86 (2000).
[20]Y. Wan, "Crown structure, radiation absorption, photosynthesis and transpiration," Ph.D. dissertation, University of Edinburgh, Edinburgh, U.K., 1988.
[21]T. Van Renterghem, E. Salomons, and D. Botteldooren, "Efficient FDTD-PE model for sound propagation in situations with complex obstacles and wind profiles," Acust. Acta Acust. **91**, 671–679 (2005).
[22]D. Duhamel, "Efficient calculation of the three-dimensional sound pressure field around a noise barrier," J. Sound Vib. **197**, 547–571 (1996).
[23]R. Blumrich and D. Heimann, "A linearized Eulerian sound propagation model for studies of complex meteorological effects," J. Acoust. Soc. Am. **112**, 446–455 (2002).
[24]V. Ostashev, D. Wilson, L. Liu, D. Aldridge, N. Symons, and D. Marlin, "Equations for finite-difference, time-domain simulation of sound propagation in moving inhomogeneous media and numerical implementation," J. Acoust. Soc. Am. **117**, 503–517 (2005).
[25]D. Botteldooren, "Finite-difference time-domain simulation of low-frequency room acoustic problems," J. Acoust. Soc. Am. **98**, 3302–3308 (1995).
[26]T. Van Renterghem and D. Botteldooren, "Prediction-step staggered-in-time FDTD: an efficient numerical scheme to solve the linearised equations of fluid dynamics in outdoor sound propagation," Appl. Acoust. **68**, 201–216 (2007).
[27]K. Gilbert and X. Di, "A fast Green's function method for one-way sound propagation in the atmosphere," J. Acoust. Soc. Am. **94**, 2343–2352 (1993).
[28]E. Salomons, "Improved Green's function parabolic equation method for atmospheric sound propagation," J. Acoust. Soc. Am. **104**, 100–111 (1998).
[29]M. Delany and E. Bazley, "Acoustic properties of fibrous absorbent materials," Appl. Acoust. **3**, 105–116 (1970).
[30]S. Tang and P. Ong, "A Monte Carlo technique to determine the effectiveness of roadside trees for containing traffic noise," Appl. Acoust. **23**, 263–271 (1988).
[31]J. Kragh, "Road traffic noise attenuation by belts of trees," J. Sound Vib. **74**, 235–241 (1981).
[32]M. Martens, "Foliage as a low-pass filter: Experiments with model forests in an anechoic chamber," J. Acoust. Soc. Am. **67**, 66–72 (1980).
[33]D. Heimann and R. Blumrich, "Time-domain simulations of sound propagation through screen-induced turbulence," Appl. Acoust. **65**, 561–582 (2004).
[34]U. Sandberg and J. Ejsmont, *Tyre/Road Noise Reference Book* (Informex, Kisa, Sweden, 2002).